A comprehensive library of fluorescent constructs of SARS-CoV-2 proteins and their initial characterisation in different cell types

Stéphanie Miserey-Lenkei*[1,2] , **Katarina Trajkovic†[1,2]** , **Juan Martín D'Ambrosio‡[2,3]** , **Amanda J Patel§[2]** , **Alenka Čopič‡[1,3]** , **Pallavi Mathur*** , **Kristine Schauer*[4]** , **Bruno Goud*** , **Véronique Albanèse‡** , **Romain Gautier§** , **Melody Subra§** , **David Kovacs§** , **Hélène Barelli§[1,5]** and **Bruno Antonny§[1,5]**

*Department of Cell Biology and Cancer, Institut Curie, PSL Research University, Sorbonne Université, CNRS, UMR144, Paris F-75005, France, †Mediterranean Institute for Life Sciences (MedILS), Split 21000, Croatia, ‡Institut Jacques Monod, Université de Paris, CNRS, UMR7592, Paris F-75006, France, and §Institut de Pharmacologie Moléculaire et Cellulaire, Université Côte d'Azur et CNRS, UMR7275, Valbonne F-06560, France

Background Information. Comprehensive libraries of plasmids for SARS-CoV-2 proteins with various tags (*e.g.*, Strep, HA, Turbo) are now available. They enable the identification of numerous potential protein–protein interactions between the SARS-CoV-2 virus and host proteins.

Results. We present here a large library of SARS CoV-2 protein constructs fused with green and red fluorescent proteins and their initial characterisation in various human cell lines including lung epithelial cell models (A549, BEAS-2B), as well as in budding yeast. The localisation of a few SARS-CoV-2 proteins matches their proposed interactions with host proteins. These include the localisation of Nsp13 to the centrosome, Orf3a to late endosomes and Orf9b to mitochondria.

Conclusions and Significance. This library should facilitate further cellular investigations, notably by imaging techniques.

Additional supporting information may be found online in the Supporting Information section at the end of the article.

---

[1]To whom correspondence should be addressed: (email: smiserey@curie.fr, katarina.trajkovic@medils.hr, alenka.copic@ijm.fr, barelli@ipmc.cnrs.fr, antonny@ipmc.cnrs.fr)

[2]These are the co-first authors.

[3]Present address: Montpellier Cell Biology Research Center, CNRS & Université de Montpellier, UMR 5237,1919 route de Mende, 34293 Montpellier, France.

[4]Present address: Inserm U1279, Gustave Roussy Institute, Université Paris-Saclay, Villejuif, France.

[5]These are the co-last authors.

Additional supporting information may be found in the online version of this article at the publisher's web-site.

Introduction

As most RNA viruses, SARS-CoV-2 virus utilises multiple protein–protein interactions with host factors to subvert cellular functions. Notably, SARS-CoV-2 infection and replication involve the sequential use of several organelles of the endocytic and secretory pathways (Sicari et al., 2020). These include interaction of the viral Spike protein with cell

receptors and its cleavage by the proteases for virion fusion with the cellular membranes (Shang et al., 2020), subversion of the endoplasmic reticulum (ER) membrane to promote the formation of the replication organelle (Klein et al., 2020), interaction with the ER–Golgi intermediate compartment for virion formation (Klein et al., 2020) and final egress of the newly assembled virions through lysosome-like organelles (Ghosh et al., 2020).

The 30 kB genome of SARS-CoV-2 codes for 14 open reading frames. Two of them, Orf1a and Orf1ab, code for alternative long polypeptides, which give rise to 16 individual non-structural proteins (Nsp1-16) upon auto-cleavage (Bar-On et al., 2020). Some of these proteins are directly involved in replication of the viral genome, most prominently the Nsp7-8-12 replicase complex and the Nsp13 helicase (Subissi et al., 2014; Chen et al., 2020; Hillen et al., 2020). Others, such as Nsp3, 4 and 6, are transmembrane proteins that promote the formation of the replication organelle, which is a double-membrane vesicular structure (Angelini et al., 2013; Oudshoorn et al., 2017; Snijder et al., 2020). Four Orfs code for the structural proteins of the virions: spike (S), which binds surface receptors on cells (angiotensin-converting enzyme 2), nucleocapsid protein (N), which is responsible for genome packaging, and two membrane proteins (E and M). A set of very small Orfs code for polypeptides involved in the final steps of virion formation (*e.g.*, Orf3a and Orf9b).

Affinity-based techniques coupled to mass spectrometry have enabled the identification of putative host cell targets of SARS-CoV-2 proteins (Gordon et al., 2020a; Stukalov et al., 2020). In one study, 26 proteins of SARS-CoV-2 virus have been cloned as Strep fusions and individually expressed in HEK293 cells, leading to the identification of about 300 potential host cell protein targets (Gordon et al., 2020a). In another study, the individual SARS-CoV-2 proteins were HA-tagged and expressed as baits in the type II pulmonary epithelial cell line A549 (Stukalov et al., 2020). In addition to identifying host protein targets of SARS-CoV-2, this study also reported changes in the host cell proteome and in post-translational modifications of the cellular proteins. To circumvent the limitation of immuno-precipitation experiments, which best capture high affinity soluble protein complexes, a second approach

based on proximity-dependent biotinylation (BioID) has been recently presented, further extending the repertoire of the interactants of the individual SARS-CoV-2 proteins (Laurent et al., 2020; St-Germain et al., 2020). A third approach employed CRISPR-Cas9 technology to knock out all putative host interactants in order to determine their effect on viral infection (Hoffmann et al., 2020). The advantage of these systematic comprehensive studies is in that they enable identification of putative druggable pathways, pointing to existing approved drugs that could be repurposed to combat the current worldwide pandemic.

Complementary information can be gained by imaging studies of the cellular localisation and dynamics of viral proteins. Given that individually expressed SARS-CoV-2 proteins interact with a number of organelle-specific proteins, it can be expected that these viral proteins might localise to and exert their function at the respective organelles. For instance, Nsp7 and Nsp13, viral proteins involved in genome replication, interact with small G proteins of the Rab family or with golgins and hence could localise to the Golgi and/or could influence Golgi morphology or function. In addition, since many SARS-CoV-2 proteins form protein complexes (*e.g.*, Nsp7/8/12; Nsp10/14) (Ma et al., 2015; Chen et al., 2020; Hillen et al., 2020), combined expression of such proteins might be necessary for *in vitro* recapitulation of their behaviour. Thus, having a repertoire of expression plasmids with different tags, including fluorescent ones, should facilitate imaging studies and cellular investigations in general.

Here, we present a large library of SARS-CoV-2 proteins tagged with either green or red fluorescent proteins and their initial characterisation in several cell lines. These lines were chosen either to mimic the cell types affected by the virus in COVID-19 patients (*e.g.*, A549, BEAS-2B and Caco-2) or for their use as established models for the understanding of basic cellular function (*e.g.*, HeLa, HEK293 and hTert-RPE1). To test for direct protein–membrane interactions or for interactions with evolutionarily highly conserved proteins, some of the SARS-CoV-2 proteins were expressed in the unicellular model *Saccharomyces cerevisiae*. In addition to assessing the localisation of individual SARS-Cov-2 proteins or protein complexes, our microscopy-based approach

Table 1 | List of the constructs

Protein	Origin	Tag Cter pEGFPN1	Tag Nter pEGFPC1	Tag Cter pmCherryN1
Nsp3	Pasteur Institute	X		X
Nsp4	UCSF Streptag II	X		X
Nsp6	Pasteur Institute	X		X
Nsp7	UCSF Streptag II	X	X	X
Nsp8	UCSF Streptag II	X	X	
Nsp10	UCSF Streptag II	X		X
Nsp12	UCSF Streptag II	X	X	
Nsp13	UCSF Streptag II	X		X
Nsp14	UCSF Streptag II	X		X
Nsp15	UCSF Streptag II		X	
ORF3a	UCSF Streptag II	X		X
ORF9b	UCSF Streptag II		X	
COV E	UCSF Streptag II		X	
COV M	UCSF Streptag II		X	

uncovers morphological and functional changes that can be induced by SARS-CoV-2 in the host cell.

Results

Construct design

All fluorescent fusion constructs were prepared from the Strep-Tag SARS-CoV-2 plasmid library described in Gordon et al. (2020a) except Nsp3, which was from a collection of SARS-CoV-2 constructs in Gateway-compatible entry vectors (Kim et al., 2020). For most proteins, we prepared both GFP and mCherry fusion constructs to facilitate co-localisation and dual expression studies (Table 1). In addition to mammalian expression vectors, we constructed plasmids for expression of SARS-CoV-2 proteins in *S. cerevisiae* (Table S1). All constructs have been deposited to *Addgene*.

We used existing structural information on the SARS-CoV-2 proteins or their SARS-CoV-1 or MERS orthologues to check the relative positions of the N- and C-termini in order to introduce the fluorescent tag on the most accessible end (Table 1). In the absence of any information or of an obvious preference, the fluorescent protein was fused at the C-terminus (Table 1). The proteins with an N-terminal tag were Nsp8, a small subunit of the replicase complex (Nsp7/8/12), Nsp15, a uridine-specific endoribonuclease essential for viral RNA synthesis, and Orf9b, a very small protein that forms a dimer in

the case of SARS-CoV (Meier et al., 2006). For the helicase Nsp13 (Hao et al., 2017), which has been suggested as a promising candidate for pharmacological targeting, we prepared both N-ter and C-ter fusion forms.

To study SARS-Cov-2 proteins in the cellular environment, we expressed single viral proteins in various cell types, including the model lung epithelial cell line A549, as well as co-expressed proteins that are known to form complexes (*e.g.*, Nsp7, Nsp8 and Nsp12) or to act together on membranes (*e.g.*, Nsp3, Nsp4 and Nsp6). Overall, the transfection efficiency and expression levels varied greatly among different constructs and sometimes among different cell lines. Some viral proteins had tendency to form aggregates and induced cytotoxicity at high expression levels. Table 2 summarises these general features.

Nsp3, Nsp4 and Nsp6

Nsp3, Nsp4 and Nsp6 are the three non-structural transmembrane proteins of the SARS-CoV-2 virus. They are involved in the formation of the replication organelle, which has the shape of a double-membrane vesicle and is derived mostly from the ER. Previous studies performed with the cognate proteins of the MERS and SARS-CoV-1 coronavirus have shown that Nsp3 and Nsp4 are necessary and sufficient for double-membrane vesicle formation, whereas Nsp6 has a facilitating role in this process (Oudshoorn et al., 2017).

In A549 cells, individually expressed Nsp3-GFP showed a characteristic ER network distribution pattern (co-localisation with the ER marker HSP90B1/Grp94/endoplasmin) with some large extensions (Figure 1A). No co-localisation was observed with autophagosome or MVB/exosome markers (Figure S1A). Individually, Nsp4-GFP and Nsp6-GFP were poorly expressed (Figure S1B). However, co-expression of Nsp3-GFP, Nsp4-mCh and Nsp6-mCh increased the expression levels for the two latter proteins. The three proteins extensively co-localised and largely affected the reticular organisation of the ER, which displayed extended structures (Figure 1B). In line with morphological changes of the ER, the staining of the ER master chaperone HSP90B1 diminished with the level of triple Nsp3/4/6 expression (Figure S1C).

Table 2 | Main expression and localisation features of the SARS-CoV-2 constructs

Protein	Function	Cell tested	Expression	Main localisation	Secondary localisation/ cellular effect	In S. cerevisiae	Figures
Nsp3	Replication organelle	A549, BEAS-2B, Caco-2, HEK293	High in A549, low in other lines	ER in A549	Toxic		1
Nsp4	Replication organelle	A549, HeLa, Caco-2, BEAS-2B, HEK293, hTert-RPE1	Very low				S1
Nsp6	Replication organelle	A549, BEAS-2B, Caco-2, HEK293	Very low in A549, high in other lines	Perinuclear structures, reticular on the periphery	Toxic		S1
Nsp3+4+6		A549	High	All on the ER	ER deformation		1
Nsp7	RdRp	A549, HeLa, Caco-2, BEAS-2B, HEK293	High	Cytosol	Puncta		2, S2
Nsp8	RdRp	A549, HeLa, Caco-2, BEAS-2B, HEK293	High	Cytosol	Puncta		2, S2
Nsp12	RdRp	A549, BEAS-2B, Caco-2, HEK293	Low	Cytosol	Golgi fragmentation		2, S2
Nsp7+8		A549		Same as alone			2
Nsp10	ExoN	A549, HeLa, Caco-2, BEAS-2B	Medium	Cytosol	Toxic	endocytic puncta	3, 4, S3
Nsp14	ExoN	A549, HeLa, Caco-2, BEAS-2B, HEK293	Very low	Cytosol		cytosol	3, 4, S3
Nsp10+14				Cytosol	Puncta		3, 4
Nsp13	Helicase	A549, HeLa, Caco-2, BEAS-2B, HEK293	Very low to low	Cytosol	Centrosome and Golgi/Golgi fragmentation	cytosol	5, S4
Nsp15		A549	High	Cytosol		Cytosol	S5
ORF3a		A549, HeLa, Caco-2, BEAS-2B, hTert-RPE1	High	Late endosomes	Toxic at high expression levels	Vacuole and ER	6, S6
ORF9b		A549, HeLa, Caco-2, BEAS-2B, hTert-RPE1	High	Mitochondria	Cytosol	Cytosol	7, S7
ORF3a+9b			High	Same as alone			7
E	Envelope protein	A549, HeLa, Caco-2, BEAS-2B	High	ER	Toxic		8, S8

Nsp7, Nsp8 and Nsp12

Nsp12 with its accessory subunits Nsp7 and Nsp8 is a central SARS-CoV-2 enzyme responsible for the replication and transcription of the viral genome through its RNA-dependent RNA polymerase (RdRp) activity. According to the previously solved structure of the replicase complex, Nsp12 forms a stoichiometric complex with one Nsp7 and two Nsp8 subunits (Chen et al., 2020; Hillen et al., 2020). Interactome studies in HEK293 cells showed that individually expressed Nsp7 interacted with numerous host proteins including multiple members of the Rab GTPase family (Gordon et al., 2020a). We expressed Nsp7, Nsp8 or Nsp12 fused with GFP or mCherry at their N or C-termini in A549 cells (Figure 2A) as well as in other cell lines (BEAS-2B,

Caco-2, HEK293, HeLa; Figure S2). All fusion proteins appeared essentially cytosolic although some small puncta were occasionally observed (Figures 2A and S2). Some Golgi fragmentation could be observed in Nsp12-expressing cells, as demonstrated by the Golgi marker GM130 (Figure 2A). Dual expression of Nsp7-mCherry and GFP-Nsp8 (Figure 2B) or of Nsp7-mCherry and Nsp12-GFP (Figure 2B) did not affect the localisation patterns of these proteins as compared with their single expressions.

Nsp10 and Nsp 14

Nsp14 is a bifunctional enzyme composed of an exonuclease domain and a SAM-dependent methyl-transferase domain (Ma et al., 2015). It forms a complex with Nsp10, a zinc-finger protein of 139

Figure 1 | Nsp3, Nsp4 and/or Nsp6 fluorescent fusions in A549 cells

(**A**) Co-localisation of Nsp3-GFP with the ER markers HSP90B1 in A549 cells. (**B**) Co-localisation of Nsp3-GFP with Nsp4-mCherry and Nsp6-mCherry in A549 cells. The ER appears either intact (upper row) or deformed into patchy structures (lower rows). (**C**) Some cells expressing high level of Nsp3-GFP, Nsp4-mCherry and Nsp6-mCherry lose proper HSP90B1 staining. All images were acquired with a confocal microscope and were analysed using Volocity software. Representative Z projections images from three different experiments. Scale bars: 10 μm, 1 or 2 μm (zoomed images).
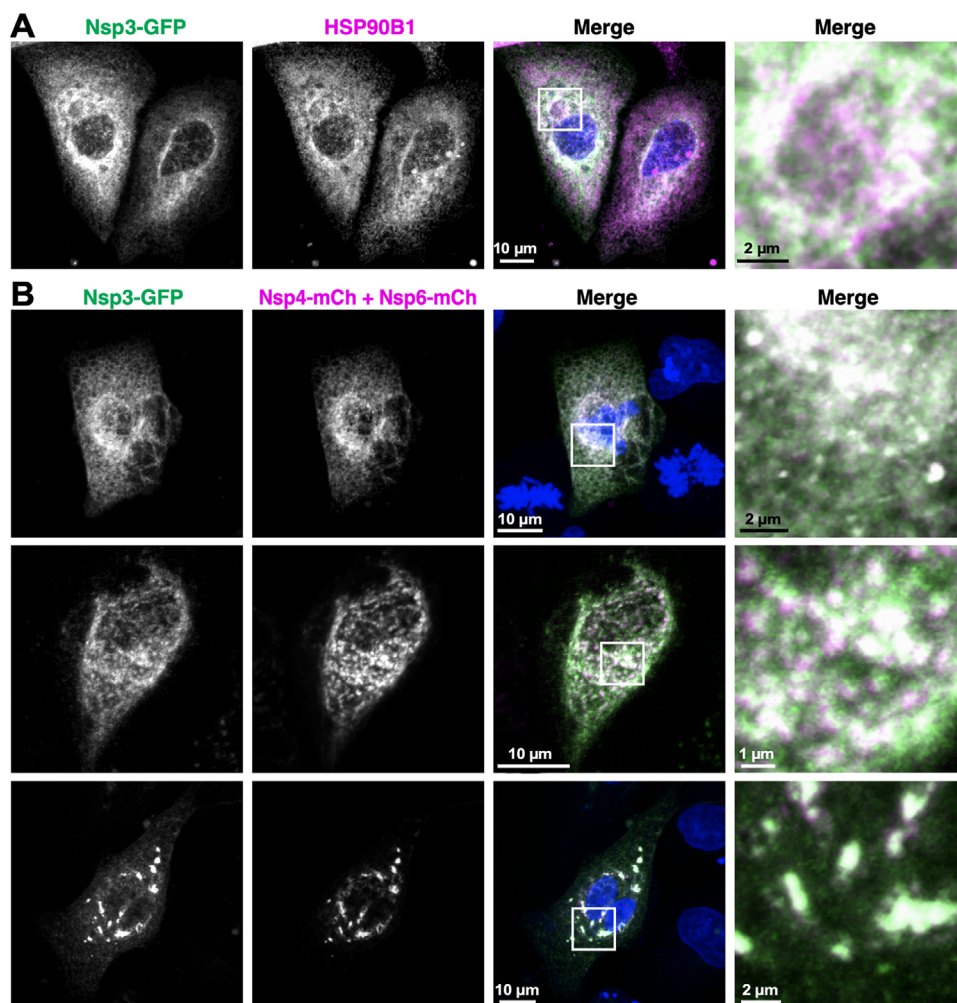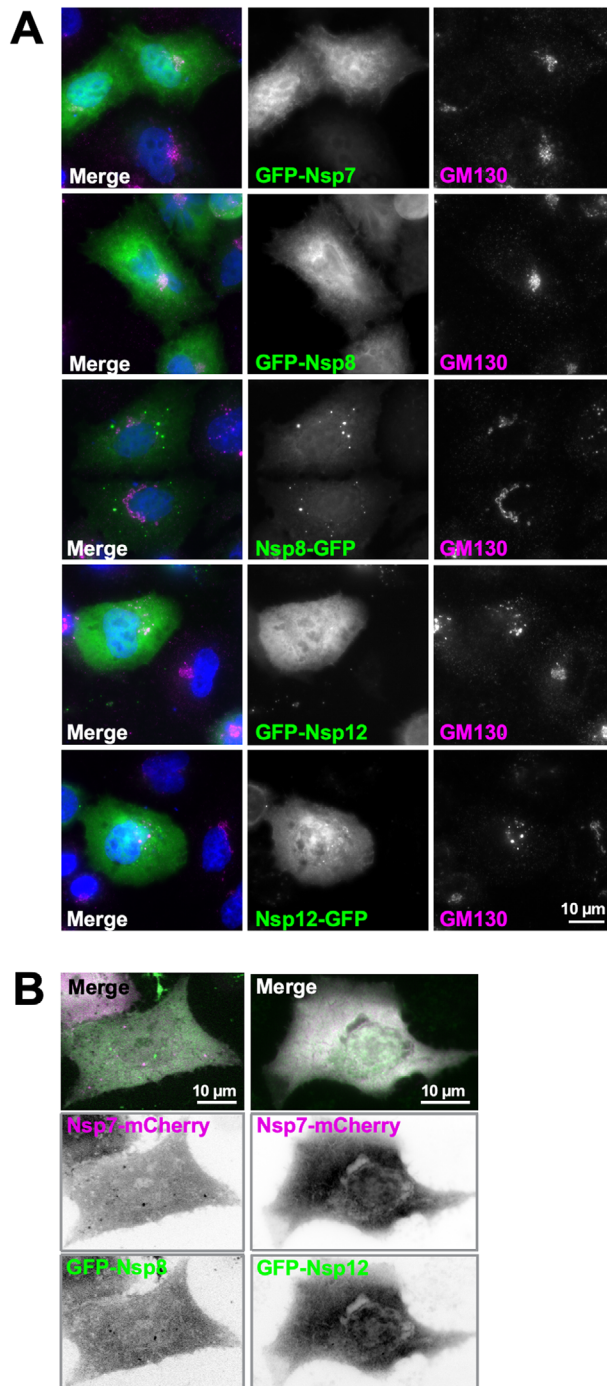

amino acids that is required for viral replication. Nsp10 has been proposed to interact with the clathrin-AP2 machinery and the ERGIC network. We expressed Nsp10-GFP and/or Nsp14-mCherry in A549 cells (Figure 3), in other mammalian cell lines (Figure S3A), or in yeast (Figure 4). In mammalian cells, individually expressed Nsp10-GFP or Nsp14-mCherry appeared mostly cytosolic (Figures 3A and S3A and S3B). When co-expressed, Nsp10-GFP and Nsp14-mCherry remained mostly

cytosolic with slight co-localisation with clathrin (Figure 3B, arrow) but no obvious co-localisation with the Ergic-53 marker (Figure S3C), although large structures and puncta positive for the two proteins could be observed (Figures 3B and S3C).

In the yeast *S. cerevisiae*, Nsp10-GFP displayed a punctate pattern (Figure 4A). Some yeast cells displayed bright and heterogeneous Nsp10-GFP puncta, which may represent protein aggregates. Other cells with a higher cytosolic signal showed

puncta that were smaller, more uniform and localised close to the cell cortex. This pattern was not influenced by co-expression of Nsp14-mCherry, which was only cytosolic (Figure 4A). The cortical Nsp10-GFP puncta resembled endocytic patches; indeed, they showed partial co-localisation with endocytic proteins Ede1 and Sac6 (Kaksonen et al., 2005), but not with TGN or endosomal markers (Figure 4B). Moreover, time-lapse imaging revealed that the Nsp10-GFP puncta were highly mobile and moved partly together with Ede1 (Figure 4B). This phenotype might indicate an interaction between Nsp10 and an evolutionary-conserved feature of the clathrin machinery.

Nsp13

The analysis of the SARS-CoV-2 interactome in HEK293 cells revealed that the helicase Nsp13 interacted with a number of Golgi-associated proteins (golgins) as well as with centrosomal proteins (Gordon et al., 2020a). We found that Nsp13-GFP was mostly cytosolic in A549 cells (Figure 5A) as well as in all tested cells including yeast (Figures S4A and S4B). However, a fraction of Nsp13-GFP clearly associated with the centrosome as visualised by anti-gamma tubulin or anti-FGFR1OP antibodies (Figure 5A). In a few cells, we observed faint co-localisation of Nsp13-GFP or Nsp13-mCherry with Golgi markers (Figure 5B, arrow heads). In addition, the expression of Nsp13 strongly affected the Golgi structure in some cells, with fragmentation of the cis, median, and trans side as assessed by Golgi markers GM130, GalNacT2 and TGN46, respectively (Figures 5B and S4C). Altogether, these cell localisation studies on Nsp13 underscore the relevance of its interactions with centrosome and Golgi proteins suggested by both affinity- and proximity-based interactome approaches (Laurent et al., 2020; Gordon et al., 2020a).

Nsp15

Nsp15 is an endonuclease that cleaves single- or double-strand RNAs after uridines (Subissi et al., 2014; Kim et al., 2020). In proteomic analysis, Nsp15 has been shown to interact with Arf6 (Gordon et al., 2020a), a small G protein that resides at the plasma membrane and on endocytic structures. However, this interaction was not confirmed by proximity-based approaches.

Figure 3 | **Nsp10 and/or Nsp14 fluorescent fusions are soluble in mammalian cells**

(**A**) Individually expressed Nsp10-GFP and Nsp14-mCherry are cytosolic in A549 cells. (**B**) Co-expressed Nsp10-GFP and Nsp14-mCherry remained mostly cytosolic with slight co-localisation with clathrin (arrow heads) but no obvious co-localisation with the ERGIC-53 marker. Large structures and puncta positive for the two proteins could also be observed (arrow heads). All images were acquired with a confocal microscope and were analysed using Volocity software. Representative Z projections images from three different experiments. Scale bars: 10 μm, 2 μm (zoomed images).
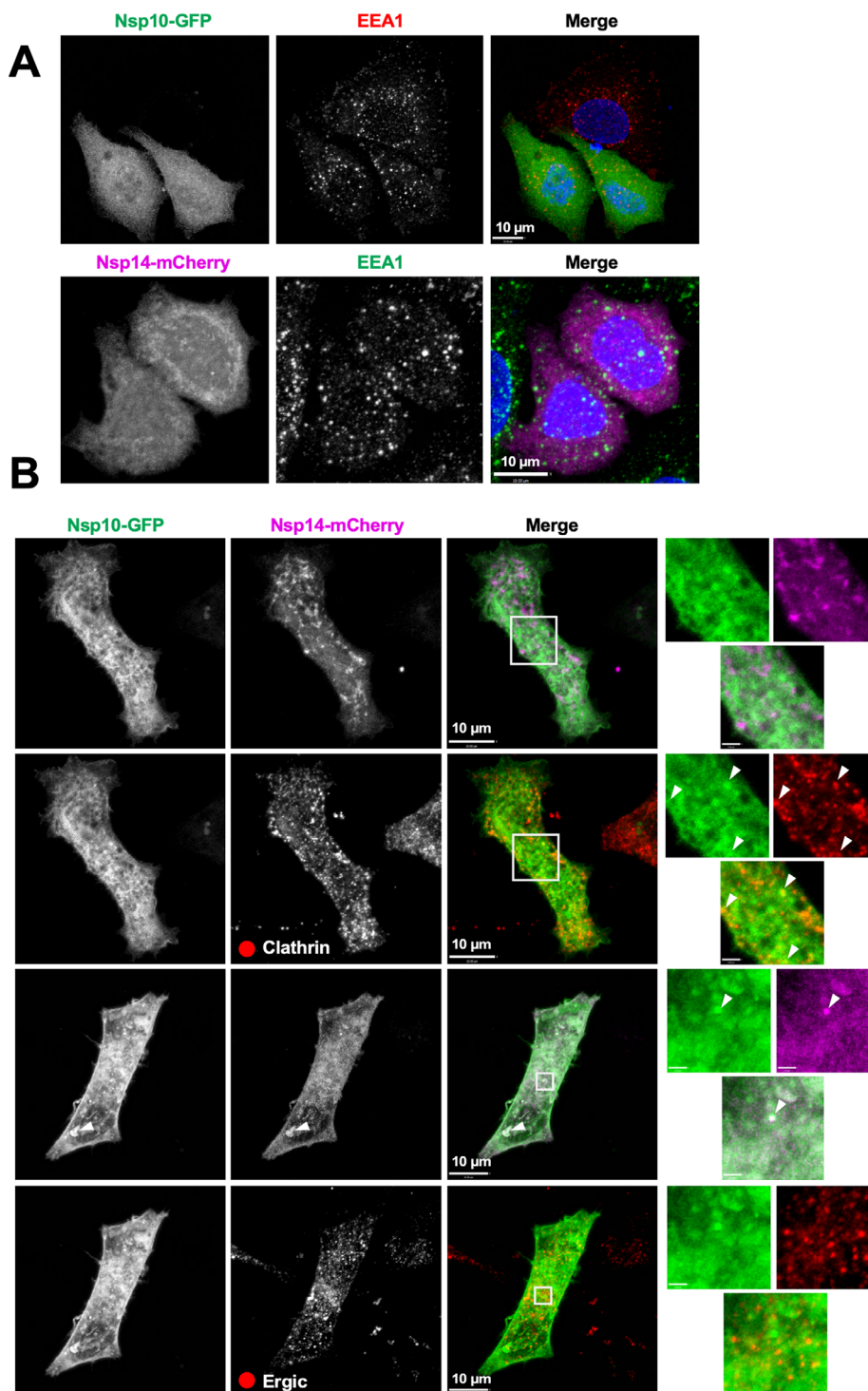
Figure 4 | Nsp10-GFP co-localises with endocytic markers in yeast

(**A**) In *S. cerevisiae* individually expressed Nsp10-GFP forms puncta, whereas Nsp14-mCherry is cytosolic. These features are preserved when Nsp10-and Nsp14-mCherry are co-expressed. (**B**) Some Nsp10-GFP puncta are dynamic and are positive for the endocytic markers epsin (Ede1-mRuby) or Sac6-mRuby. Imaging: spinning disk microscopy; bars = 3 μm.
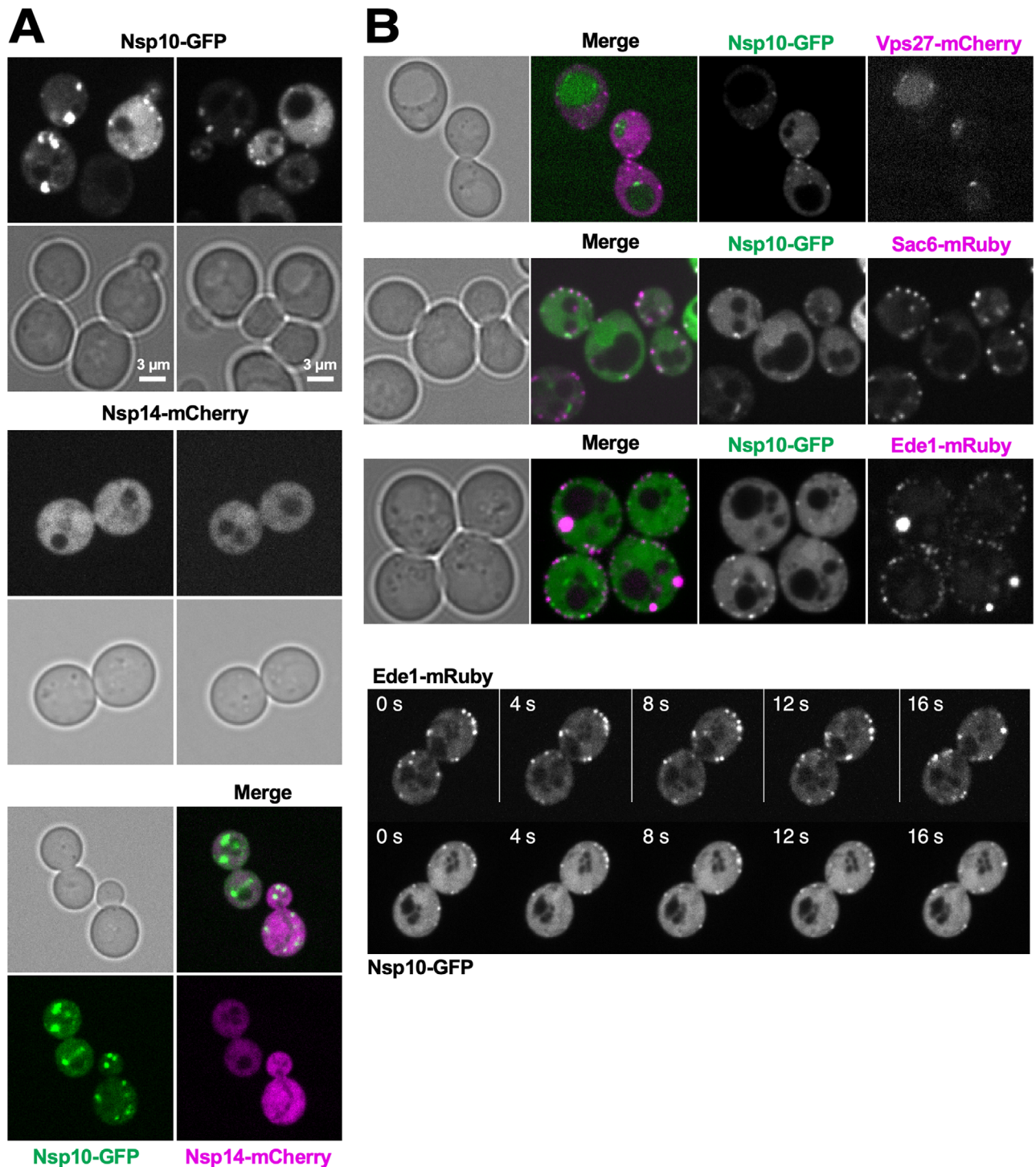
Figure 5 | Nsp13-GFP is mostly soluble but a fraction co-localises with the centrosome
(**A**) In A549 cells, Nsp13-GFP is mostly cytosolic but a fraction associates with the centrosome as revealed by antibodies against gamma tubulin or FGFR1OP. (**B**) In some cells expressing Nsp13-GFP, Golgi markers become scattered (arrow heads), showing a fragmentation of the Golgi apparatus. All images were acquired with a confocal microscope and were analysed using Volocity software. Representative Z projections images from four different experiments. Scale bars: 10 μm, 2 μm (zoomed images).
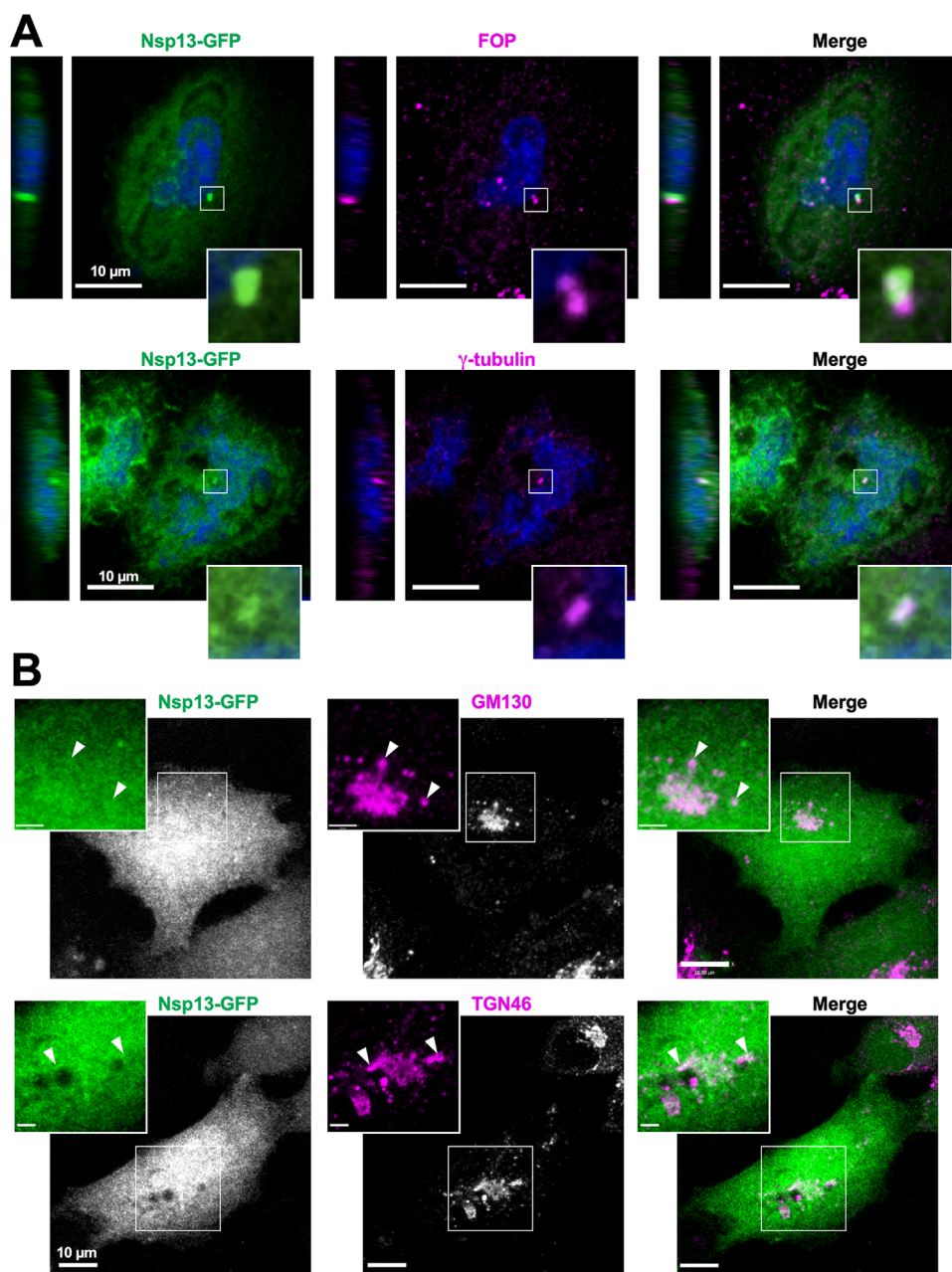
In our experiments, Nsp15 was found cytosolic in A549 cells (Figure S5A) as well as in yeast (Figure S5B).

Orf3a

Orf3a contains three transmembrane helices followed by a long cytosolic tail containing a Yxxø endocytic

motif (Tan et al., 2004). Orf3a self-assembles as a dimer in lipid membranes, forming a non-selective cation channel (Kern et al., 2020). In all tested mammalian cell lines, we observed a vesicular pattern of Orf3a-mCherry (Figures 6A–6D and S6A). In A549 cells, Orf3a-mCherry co-localised with late endocytic compartments (Figures 6A, 6B and S6B). These compartments were highly mobile, as assessed by time-lapse multicolour imaging (Figure 6B; arrows, bottom panel). Orf3a-mCherry also partly co-localised with GM130 (Golgi marker) as well as LC3 (autophagosome marker) (Figure 6C), in line with recent work showing that Orf3a changes the balance between autophagosome formation and autophagosome maturation (Qu et al., 2020). Late endosomal and Golgi localisation of Orf3a is in agreement with studies on Orf3a of the related SARS-CoV-1 virus (Freundt et al., 2010; Yue et al., 2018). Interestingly, Orf3a-mCherry expression led to changes in endosomal morphology, with enlargement not only of Orf3a-containing late endosomes, but also of the early endosomes that did not co-localise with Orf3a (Figures 6D and S6C). These data suggest possible perturbation of the entire endocytic pathway by Orf3a.

The preference of Orf3a for late endosomal compartment was preserved even in yeast, where Orf3a-mCherry could be observed decorating the vacuolar membrane (as revealed with Vph1-GFP) (Figure 6E). Some Orf3a was also observed at the ER (visualised by Sec63-GFP; Figure 6E) but not at the Golgi (Sec7-GFP; Figure S6D) and at Golgi-to-vacuole transport intermediates (Vps17-GFP; Figure S6D). We suspect that some Orf3a was retained in the ER due to difficulties in folding. In agreement, the localisation of Orf3a largely shifted towards the vacuole in aged yeast cells, and we observed no co-localisation with lipid droplets (Figure S6D).

Orf9b

SARS-CoV-2 Orf9b-GFP fusion protein displayed a typical mitochondrial pattern in all tested cell lines (A549, BEAS-2B, Caco-2 and HeLa) (Figures 7A and S7A), and was specifically associated with mitochondria in A549 cells as assessed by its co-localisation with the mitochondrial marker Tom20 (Figure 7A), Mitotracker and DsRed-Mito-7 (Figure S7B), similarly to what has been described for the cognate protein Orf9b from SARS-CoV-1 (Shi et al.,

2014). Recent investigations indicate that Orf9b from SARS-CoV-2 interacts with the mitochondrial protein TOM70 (Jiang et al., 2020; Kreimendahl and Rassow, 2020). Consistent with this observation, mutating an Orf9b residue in the interacting region with TOM70 (Gordon et al., 2020) (L52D) abolished the mitochondrial localisation of Orf9b (Figures 7A and S7C). We also noticed that the mitochondrial fraction of Orf9b decreased when it was expressed at a higher level. This effect was probably due to titration of endogenous TOM70 by over-expressed Orf9b at the mitochondria surface.

We then co-expressed Orf3a-mCherry and Orf9b-GFP aiming to see whether they influence each other's localisation. The combined expression of the two proteins did not change their overall localisation patterns as compared with single expressions, although we did observe motile structures co-labelled with the two markers by time-lapse multicolour imaging (Figure 7B, arrows).

Because the structure of isolated Orf9b strongly differs from the structure of Orf9b in complex with TOM70 and a direct mechanism for lipid membrane recognition has been suggested (Meier et al., 2006), we next tested whether Orf9b associated with mitochondria via protein–protein or protein–lipid interactions. To this end, we expressed Orf9b-GFP in *S. cerevisiae*, which harbours a TOM70 protein homologue (Chan et al., 2006; Kreimendahl and Rassow, 2020). Here, Orf9b-GFP appeared entirely soluble (Figure 7C), suggesting that mitochondrial localisation of Orf9b relies on a specific interaction between Orf9b and human TOM70 and not on direct interaction with the lipid bilayer.

Envelope protein (E)

Protein E is a very short (75 aa) single-pass transmembrane protein, which forms a pentameric ion channel in lipid membranes, thereby acting as a viroporin (Mandala et al., 2020). E proteins of other coronaviruses function in viral assembly and release. To reduce interference in protein E trafficking, which involves motifs in its C-terminal cytosolic part, we fused GFP to the short N-terminal luminal region of protein E. In all tested cell lines and even at low level of expression, SARS-CoV-2 GFP-E showed reticular pattern (Figure S8A) and co-localised with ER markers in A549 cells (Figure 8 and S8B). We also observed deformation of the ER

Figure 6 | Fluorescent-fusion forms of Orf3a localises to late endocytic compartments in mammalian cells and in yeast
(**A**) A549 cells expressing Orf3a-mCherry were immunolabelled with an antibody against the late endosomal markers Lamp1 and imaged by wide-field microscopy. (**B**) Real-time spinning disk microscopy of A549 cells co-expressing Orf3a-mCherry and Lamp1-GFP. Pictures were acquired at the indicated time. Higher magnifications of the images are shown. Arrows point to a moving structure where Orf3a-mCherry and Lamp1-GFP are co-localised. (**C**) A549 cells were transfected with Orf3a-mCherry and stained with the Golgi marker GM130 and the autophagosome marker LC3. Higher magnifications of the images are shown. (**D**) Wide-field images of A549 cells transfected with Orf3a-mCherry and analysed by immunofluorescence for endosomal markers. The cells expressing Orf3a showed enlarged endocytic structures as compared with naïve cells. (**E**) Spinning disk microscopy images of *S. cerevisiae* cells expressing Orf3a-mCherry. The fluorescent construct shows strong co-localisation with a vacuole marker (Vph1-mCherry) and moderate co-localisation with an ER marker (Sec63-GFP). Bars = 10 μm (A–D) or 3 μm (E).
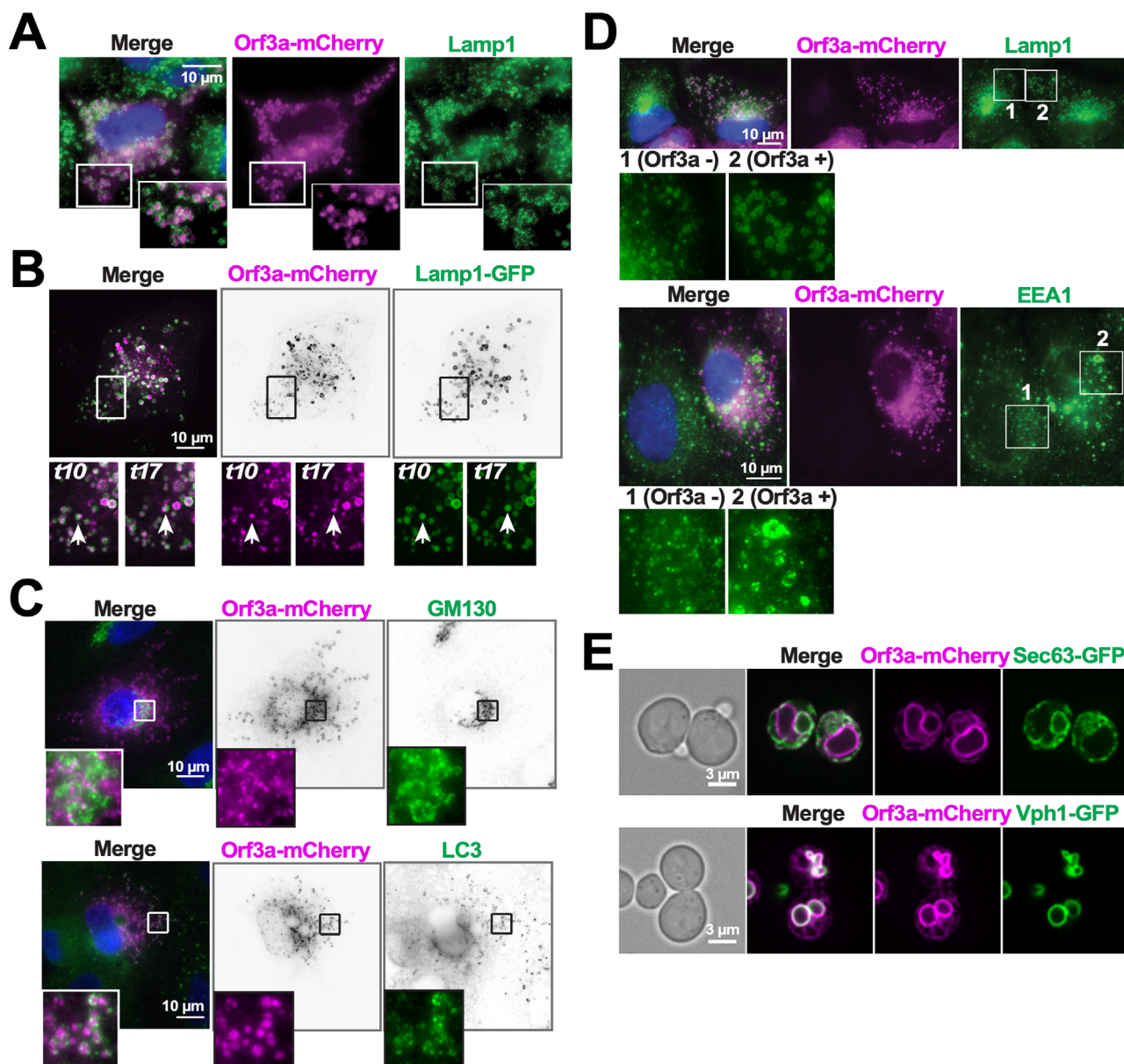
Figure 7 | Orf9b-GFP localises to mitochondria in mammalian cells
(**A**) A549 cells were transfected with Orf9b-GFP or Orf9b-L52D-GFP mutant and immunolabeled with the mitochondrial marker Tom20. Representative images are shown. (**B**) A549 cells were co-transfected with Orf9b-GFP and Orf3a-mCherry and imaged using time-lapse multicolour imaging. Real time pictures were acquired using a spinning disk microscope and pictures were acquired at the indicated time. Higher magnifications of the images are shown. Arrows point to a moving structure where Orf3a-mCherry and Orf9b-GFP co-localise (**C**). In *S. cerevisiae* Orf9b-GFP is soluble. Bars: 10 μm (A and B) and 3 μm (C).
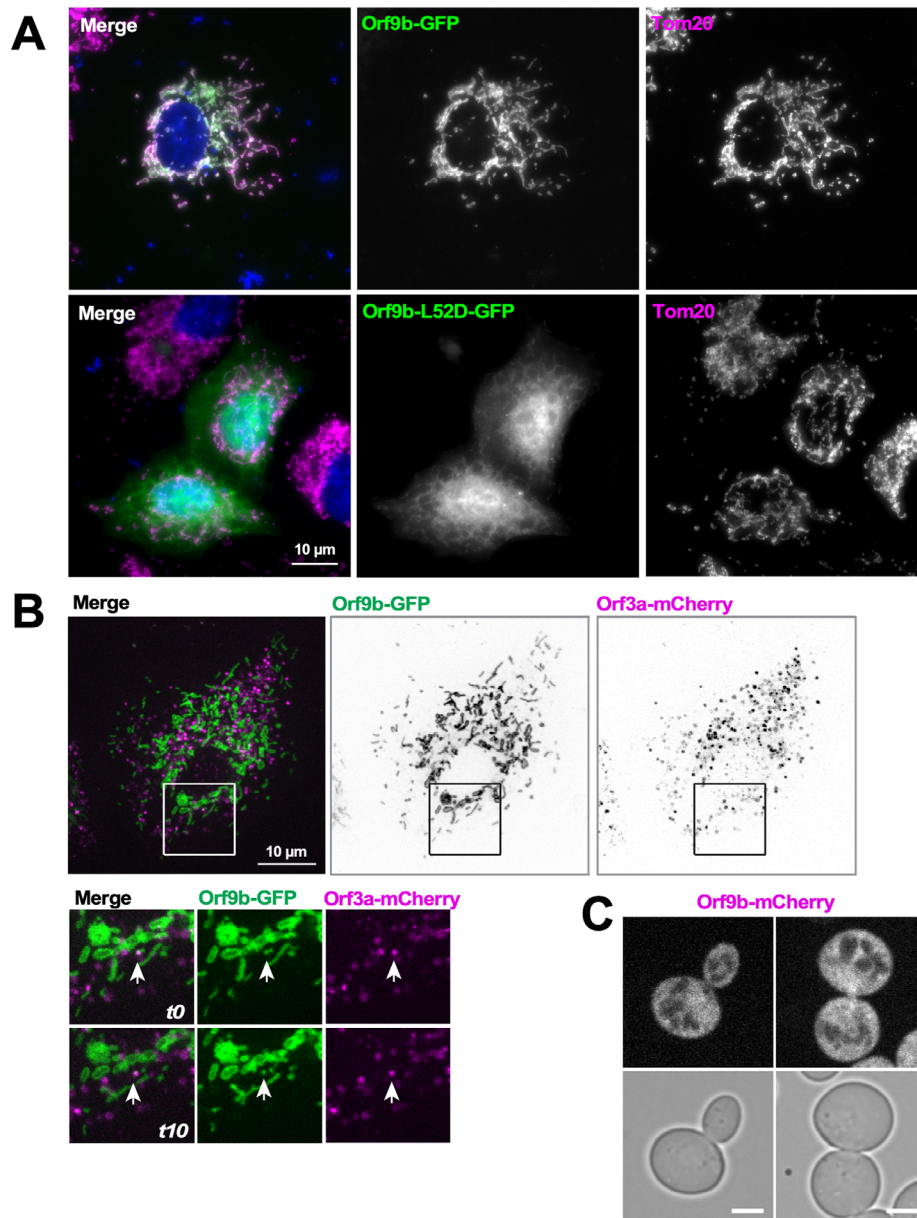

and cytotoxicity in cells expressing high levels of SARS-CoV-2 E protein. Given the very small size of E and its tight pentameric structure, we cannot exclude that the GFP moiety affects its assembly and trafficking fate. Recent studies indicate an interplay between E, S and M proteins of SARS-CoV-2 for their trafficking and maturation (Boson et al., 2021).

Figure 8 | SARS-CoV-2 E protein localises to ER

Wild-field microscopy images showing co-localisation of GFP-E with the ER marker DsRed2-ER-5 in A549 cells. Bar: 10 μm.
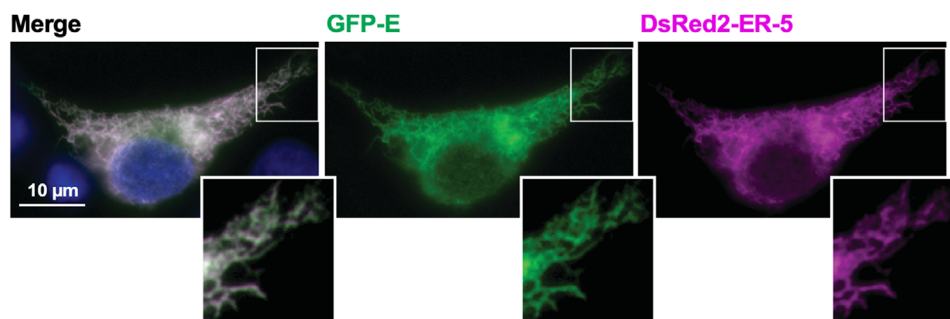
Discussion

The identification of potential interactions between individual SARS-CoV-2 proteins and mammalian proteins by affinity- or proximity-based proteomic analysis (Laurent et al., 2020; St-Germain et al., 2020; Stukalov et al., 2020; Gordon et al., 2020a) suggests hypothesis for the cellular pathways that might be targeted to interfere with viral infection or replication. The fluorescent constructs generated and described in this study should aid at exploring these interactions in different cellular context, should it be at the scale of individual proteins or in more integrated studies with several viral proteins working in concert. Of note, SARS-CoV-2 constructs with a Flag tag and thus suitable for immunofluorescence are now also available (Zhang et al., 2020). We used our preliminary microscopy observations with some of the SARS-CoV-2 fluorescent constructs to test the relevance of some of the reported interactions, notably with regard to the attachment to or remodelling of membrane compartments. Because the general features of the secretory pathway are conserved in eukaryotes, we also tested the localisation of some SARS-CoV-2 proteins in budding yeast. Figure 9 summarises our major observations. The cellular localisation of a few SARS-CoV-2 proteins is in agreement with previous proteomic studies (e.g., Nsp13, Orf9b). However, many SARS-CoV-2 fluorescent fusions appear essentially soluble.

A striking feature of the interactome map of individual SARS-CoV-2 proteins is pairing of the viral proteins involved in genome replication (e.g., Nsp7 and Nsp13) with organelle-specific proteins, such as small G proteins of the Rab family, golgins or centrosomal proteins. Such interactions raise questions about the position of the replication machinery during cell infection, and most notably about the topological constraints imposed by the formation of the replication organelle on the virus replication (Snijder et al., 2020; Wolff et al., 2020). When the enzymes involved in RNA replication and transcription are encapsulated in a double-membrane vesicle, they cannot have access to other organelles. However, this consideration is not valid at other stages, when Orf1a and Orf1ab, which include the replicase complex, are themselves translated in the cytosol before formation of the double-membrane replication organelle (Snijder et al., 2020). Therefore, a temporal map of the interactions between SARS-CoV-2 and host proteins is needed.

The cell transfection experiments presented here indicate that many Nsp proteins involved in SARS-CoV-2 replication and transcription (e.g., Nsp7, Nsp8, Nsp12, Nsp15) are intrinsically soluble. A notable exception is Nsp13, which associates with the centrosome. The observations that Nsp10 co-localises with endocytic foci in yeast and that co-expressed Nsp10 and Nsp14 partially co-localised with clathrin in A549 cells are intriguing because interaction between Nsp10 and the clathrin adaptor AP-2 subunits have been observed by proteomics (Gordon et al., 2020a). It is possible that this interaction is preserved in yeast. It remains to be explored whether Nsp10 and Nsp14 affect endocytosis.

The most notable membrane interactions of the viral proteins identified in this study were those of Nsp3/4/6 and E with the ER, Orf3a with late endosomes and Orf9b with mitochondria. These

Figure 9 | General scheme of the localisation of the SARS-CoV-2 fusion proteins in mammalian cells
For the proteins tested in yeast, the agreement/disagreement with the observations made in mammalian cells is also indicated.
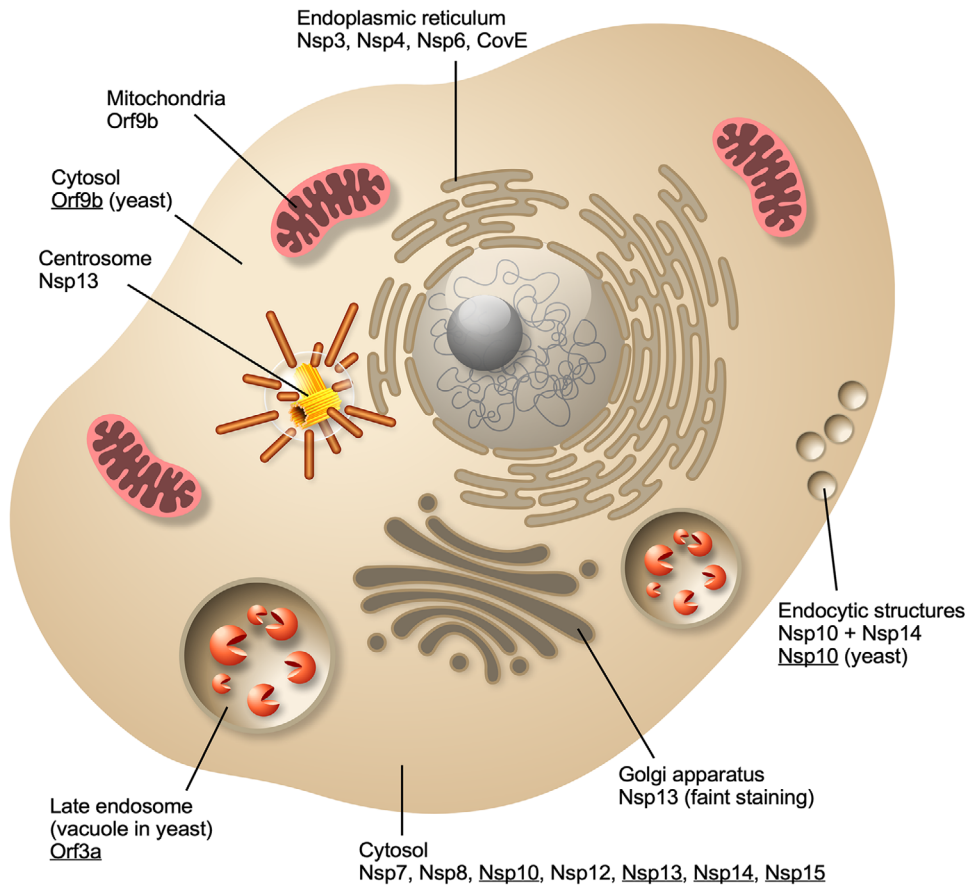
observations illustrate the complex rewiring of cellular membranes upon infection by the virus. The impact of Orf3a on late endosomal compartments in mammalian cells is particularly striking. The fact that Orf3a localises to the corresponding compartment (the vacuole) when expressed in budding yeast suggests the possibility for high-throughput drug screening assays using this simple model organism. Due to its widespread effects in cells, Orf3a has been suggested as a promising therapeutic target (Zhong et al., 2006; Kern et al., 2020).

Localisation of SARS-CoV-2 E at the ER was somewhat surprising, given that E proteins of other coronaviruses mostly localise to the ERGIC and the Golgi (Schoeman and Fielding, 2019), except for the avian infection bronchitis virus E protein, which, in addition to the Golgi, has been detected at the

ER, likely due to its C-ter retention signal (Corse and Machamer, 2000; Lim and Liu, 2001). ER localisation of SARS-Cov-2 E is unlikely to be due to protein–protein interactions since its interaction partners do not seem to include ER-resident proteins (Gordon et al., 2020a). Other possibilities include the presence of an ER-retention signal within the protein, as well as retention in the ER due to misfolding or the presence of the EGFP tag.

Several viral proteins were cytotoxic and showed specific effects on the compartment where they were localised. For instance, we observed deformations of the ER upon expression of Nsp3/4/6 and CovE and Golgi fragmentation in the presence of Nsp12 and Nsp13. Interestingly, in cells expressing late endosome-localised Orf3a, we observed morphological alterations not only in late, but also in early

endosomes, suggesting that at least some viral proteins may exert wide-spread effects beyond their immediate vicinity in the cell.

Materials and methods

Mammalian cell expression
A549, HeLa, HEK293, Caco-2, BEAS-2B and hTert-RPE1 cell lines were used for testing the localisation of SARS-Cov-2 proteins. All cell lines were maintained in Dulbecco's Modified Eagle Medium or in DMEM/F12 (Gibco) supplemented with 10 % foetal calf serum. Transfections were done using Lipofectamine 2000 (Thermofisher) or Lipofectamine 3000 (Invitrogen) according to the manufacturer's instructions. Media was replaced 6 hours post-transfection and cells were incubated for a total of 24 or 48 h.

Yeast manipulations, strains and plasmid construction
Yeast manipulations were performed using standard methods and growth conditions (Dunham and Gartenberg, 2015). All plasmids used in this study are listed in Table S1. In-Fusion HD Cloning Plus kit (Takara Bio) was used according to the supplier instructions. Briefly, individual PCR products corresponding to coding sequences of the viral proteins (Nsp10, Nsp13, Nsp14, Nsp15, Orf3a and Orf9b) were cloned into a low-copy (CEN) plasmid containing the medium-strength ADH1-promotor and a gene for fluorescent protein (C-ter-GFP, N-ter-mCherry or C-ter-mCherry), upon linearisation by a restriction enzyme. All resulting plasmids were verified by DNA sequencing. Plasmids were transformed either into a wild-type yeast strain or, for co-localisation analyses, into strains expressing endogenously tagged yeast proteins. Yeast strains are listed in Table S2. Gene chromosome-tagging was performed by homologous recombination and confirmed by PCR on genomic DNA. The tagging with mRuby2 was performed using the plasmid pFa-mRuby::HIS5 (Lee et al., 2013).

Immunofluorescence
Cell fixation was performed with 3% or 4% paraformaldehyde (Electron Microscopy Sciences) for 15 min at room temperature or with methanol for 2 min at −20°C. For permeabilisation, cells were incubated in PBS supplemented with 2 g/l BSA and 0.5 g/l saponin for 10 min at room temperature. For staining with antibodies against EEA1, Lamp1, M6PR and calnexin, cells were permeabilised with 0.05 % Triton X-100 in PBS for 5 min at room temperature.

Primary antibodies used in this study were mouse anti-GM130 (BD Biosciences; ref 610823 and Roche, ref 11814460001), rabbit anti-GalNacT2 (Sigma; HPA01122), sheep anti-TGN46 (Biorad; ahp500g), mouse anti ERGIC-53 (Santa Cruz; sc-398777), mouse anti-HSP90B1 (Sigma; AMAb91019), rabbit anti-Tom20 (Santa Cruz; sc-11415), mouse anti-EEA1 (BD Transduction Laboratories; 610456 or 610457), anti-Lamp1 (Santa Cruz; sc-20011), anti-M6PR (Abcam; ab134153), anti-calnexin (Millipore; MAB 3126), mouse anti-Tsg101 (GeneTex; GTX70255). Mouse anti-clathrin antibodies were a kind gift from Michel Franco. Mitochondria were labelled using Mitotracker™ Red CMX Ros (Invitrogen; M7512). For co-localisation studies, particular organelles were visualised by co-expressing fluorescent organelle markers (Rab7-GFP (Addgene #28047), DsRed2-Mito-7 (Addgene #55838) or DsRed2-ER-5 (Addgene #55836)). Alexa-Secondary antibodies were purchased from Jackson ImmunoResearch Laboratory.

Coverslips were mounted in Mowiol and examined with the following microscopes:

(1) An inverted LSM780 confocal microscope (Carl Zeiss, France) equipped with a 63X oil immersion objective lens (numerical aperture NA 1.4). Z-series of 16–20 images were compressed into two dimensions using the maximum projection of Volocity software (Figures 1, 3, 5, S1, S3B, S3C, S4C and S5A).
(2) A 3D deconvolution microscope (Leica DM-RXA2), equipped with a piezo z-drive (Physik Instrument) and a 100×1.4NA-PL-APO objective lens for optical sectioning. 3D or 1D multicolour image stacks were acquired using the Metamorph software (MDS) through a cooled CCD-camera (Photometrics Coolsnap HQ) (Figures 2A, 2B, 6C and 7A).
(3) A Zeiss Axio Observer microscope with a EC Plan NEOFLUAR 100x/1.3 Oil Ph3 objective. Images were acquired by a Zeiss Axiocam 506 mono camera using a ZEN blue software (Figures S2, S3A, S4A, 6A, 6D, S6A–S6C, S7, 8 and S8).

Live cell imaging of the mammalian cells
Spinning-disk confocal time-lapse imaging was done at 37°C in a thermostat-controlled chamber using an Eclipse 80i microscope (Nikon) equipped with spinning disk confocal head (Perkin), a 100x objective and either a Ultra897 iXon camera (Andor) or CoolSnapHQ2 camera (Roper Scientific). Corresponding time-lapse images are displayed in Figures 2B, 6B and 7B.

Fluorescence microscopy in yeast
Yeast cells were grown for 14–24 h at 30°C in an appropriate minimal medium to maintain plasmid selection. Cells were harvested by centrifugation in mid-logarithmic phase (OD_{600} = 0.5–0.8) or, exceptionally, in stationary phase (OD_{600} = 4–6) and prepared for viewing on glass slides. Imaging was performed at room temperature using an Axio Observer Z1 microscope (Zeiss), equipped with an oil immersion plan apochromat 100× objective NA 1.4, an sCMOS PRIME 95 camera (Photometrics) and a spinning-disk confocal system CSU-X1 (Yokogawa). GFP-tagged proteins and mCherry- or mRuby-tagged proteins were visualised with a GFP Filter 535AF45 and an RFP Filter 590DF35, respectively. Images were acquired with MetaMorph 7 software (Molecular Devices) and processed with ImageJ (NIH, MD).

Author contribution
A.P. prepared the mammalian constructs with the help of R.G., M.S. and D.K. J.M.D. prepared the yeast constructs. H.B. analysed Nsp3, Nsp4, Nsp6, Nsp10, Nsp13, Nsp14, Nsp15 constructs in A549 by confocal microscopy. S.M.L. analysed Nsp7, Nsp8, Nsp12, Orf3a and Orf9b in A549 with the help

of P.M. and K.S. by 3D- and live-cell imaging. M.S. analysed Nsp4 and Nsp6 in RPE1 cells. K.T. analysed the constructs in different mammalian cell lines by wide-field fluorescence microscopy. J.M.D. and A.C. analysed the constructs in yeast cells by spinning-disk microscopy. V.A. contributed yeast strains and participated in yeast project design. B.A., H.B., A.C., B.G., S.M.L., A.P., K.S. and K.T. wrote and edited the manuscript. B.A. coordinated the project.

Conflict of interest statement

The authors have declared no conflict of interest.

References

Angelini, M. M., Akhlaghpour, M., Neuman, B. W. and Buchmeier, M. J. (2013) Severe acute respiratory syndrome coronavirus nonstructural proteins 3, 4, and 6 induce double-membrane vesicles. mBio **4** (4), e00524-13. https://doi.org/10.1128/mBio.00524-13.

Bar-On, Y. M., Flamholz, A., Phillips, R. and Milo, R. (2020) SARS-CoV-2 (COVID-19) by the numbers. eLife **9**, e57309. https://doi.org/10.7554/eLife.57309.

Boson, B., Legros, V., Zhou, B., Siret, E., Mathieu, C., Cosset, F.-L., Lavillette, D. and Denolly, S. (2021) The SARS-CoV-2 envelope and membrane proteins modulate maturation and retention of the spike protein, allowing assembly of virus-like particles. J. Biol. Chem. **296**, 100111.

Chan, N. C., Likić, V. A., Waller, R. F., Mulhern, T. D. and Lithgow, T. (2006) The C-terminal TPR domain of Tom70 defines a family of mitochondrial protein import receptors found only in animals and fungi. J. Mol. Biol. **358**, 1010–1022.

Chen J., Malone B., Llewellyn E., Grasso M., Shelton P. M. M., Olinares P. D. B., Maruthi K., Eng E. T., Vatandaslar H., Chait B. T., Kapoor T. M., Darst S. A., Campbell E. A. (2020) Structural Basis for Helicase-Polymerase Coupling in the SARS-CoV-2 Replication-Transcription Complex. Cell, **182** (6), 1560–1573.e13. https://doi.org/10.1016/j.cell.2020.07.033.

Corse, E. and Machamer, C. E. (2000) Infectious bronchitis virus E protein is targeted to the Golgi complex and directs release of virus-like particles. J. Virol. **74**, 4319–4326.

Dunham, M. J., Gartenberg, M. R. & Brown, G. W. (2015) Methods in Yeast Genetics and Genomics: A Cold Spring Harbor Laboratory Course Manual.Cold Spring Harbor, NY 11724: CSHL Press,

Ghosh S., Dellibovi-Ragheb T. A., Kerviel A., Pak E., Qiu Q., Fisher M., Takvorian P. M., Bleck C., Hsu V. W., Fehr A. R., Perlman S., Achar S. R., Straus M. R., Whittaker G. R., de Haan C. A. M., Kehrl J., Altan-Bonnet G., Altan-Bonnet N. (2020) β-Coronaviruses Use Lysosomes for Egress Instead of the Biosynthetic Secretory Pathway. Cell, **183** (6), 1520–1535.e14. https://doi.org/10.1016/j.cell.2020.10.039.

Gordon D. E., Jang G. M., Bouhaddou M., Xu J., Obernier K., White K. M., O'Meara M. J., Rezelj V. V., Guo J. Z., Swaney D. L., Tummino T. A., Hüttenhain R., Kaake R. M., Richards A. L., Tutuncuoglu B., Foussard H., Batra J., Haas K., Modak M., Kim M., Haas P., Polacco B. J., Braberg H., Fabius J. M., Eckhardt M., Soucheray M., Bennett M. J., Cakir M., McGregor M. J., Li Q., Meyer B., Roesch F., Vallet T., Mac Kain A., Miorin L., Moreno E., Naing Z. Z. C., Zhou Y., Peng S., Shi Y., Zhang Z., Shen W., Kirby I. T., Melnyk J. E., Chorba J. S., Lou K., Dai S. A., Barrio-Hernandez Inigo, Memon D., Hernandez-Armenta C., Lyu J., Mathy C. J. P., Perica T., Pilla K. B., Ganesan S. J., Saltzberg D. J., Rakesh R., Liu X., Rosenthal S. B., Calviello L., Venkataramanan S., Liboy-Lugo J., Lin Y., Huang X.-P., Liu Y. F., Wankowicz S. A., Bohn M., Safari M., Ugur F. S., Koh C., Savar N. S., Tran Q. D., Shengjuler D., Fletcher S. J., O'Neal M. C., Cai Y., Chang J. C. J., Broadhurst D. J., Klippsten S., Sharp P. P., Wenzell N. A., Kuzuoglu-Ozturk D., Wang H.-Y., Trenker R., Young J. M., Cavero D. A., Hiatt J., Roth T. L., Rathore U., Subramanian A., Noack J., Hubert M., Stroud R. M., Frankel A. D., Rosenberg O. S., Verba K. A., Agard D. A., Ott M., Emerman M., Jura N., von Zastrow M., Verdin E., Ashworth A., Schwartz O., d'Enfert C., Mukherjee S., Jacobson M., Malik H. S., Fujimori D. G., Ideker T., Craik C. S., Floor S. N., Fraser J. S., Gross J. D., Sali A., Roth B. L., Ruggero D., Taunton J., Kortemme T., Beltrao P., Vignuzzi M., García-Sastre A., Shokat K. M., Shoichet B. K., Krogan N. J. (2020) A SARS-CoV-2 protein interaction map reveals targets for drug repurposing. Nature, **583** (7816), 459–468. https://doi.org/10.1038/s41586-020-2286-9.

Gordon D. E., Hiatt J., Bouhaddou M., Rezelj V. V., Ulferts S., Braberg H., Jureka A. S., Obernier K., Guo J. Z., Batra J., Kaake R. M., Weckstein A. R., Owens T. W., Gupta M., Pourmal S., Titus T. E. W., Cakir M., Soucheray M., McGregor M., Cakir Z., Jang G., O'Meara M. J., Tummino T. A., Zhang Z., Foussard H., Rojc A., Zhou Y., Kuchenov D., Hüttenhain R., Xu J., Eckhardt M., Swaney D. L., Fabius J. M., Ummadi M., Tutuncuoglu B., Rathore U., Modak M., Haas P., Haas K. M., Naing Z. Z. C., Pulido E. H., Shi Y., Barrio-Hernandez I., Memon D., Petsalaki E., Dunham A., Marrero

M. C., Burke D., Koh C., Vallet T., Silvas J. A., Azumaya C. M., Billesbølle C., Brilot A. F., Campbell M. G., Diallo A., Dickinson M. S., Diwanji D., Herrera N., Hoppe N., Kratochvil H. T., Liu Y., Merz G. E., Moritz M., Nguyen H. C., Nowotny C., Puchades C., Rizo A. N., Schulze-Gahmen U., Smith A. M., Sun M., Young I. D., Zhao J., Asarnow D., Biel J., Bowen A., Braxton J. R., Chen J., Chio C. M., Chio U. S., Deshpande I., Doan L., Faust B., Flores S., Jin M., Kim K., Lam V. L., Li F., Li J., Li Y.-L., Li Y., Liu X., Lo M., Lopez K. E., Melo A. A., Moss F. R., Nguyen P., Paulino J., Pawar K. I., Peters J. K., Pospiech T. H., Safari M., Sangwan S., Schaefer K., Thomas P. V., Thwin A. C., Trenker R., Tse E., Tsui T. K. M., Wang F., Whitis N., Yu Z., Zhang K., Zhang Y., Zhou F., Saltzberg D., Hodder A. J., Shun-Shion A. S., Williams D. M., White K. M., Rosales R., Kehrer T., Miorin L., Moreno E., Patel A. H., Rihn S., Khalid M. M., Vallejo-Gracia A., Fozouni P., Simoneau C. R., Roth T. L., Wu D., Karim M. A., Ghoussaini M., Dunham I., Berardi F., Weigang S., Chazal M., Park J., Logue J., McGrath M., Weston S., Haupt R., Hastie C. J., Elliott M., Brown F., Burness K. A., Reid E., Dorward M., Johnson C., Wilkinson S. G., Geyer A., Giesel D. M., Baillie C., Raggett S., Leech H., Toth R., Goodman N., Keough K. C., Lind A. L., Klesh R. J., Hemphill K. R., Carlson-Stevermer J., Oki J., Holden K., Maures T., Pollard K. S., Sali A., Agard D. A., Cheng Y., Fraser J. S., Frost A., Jura N., Kortemme T., Manglik A., Southworth D. R., Stroud R. M., Alessi D. R., Davies P., Frieman M. B., Ideker T., Abate C., Jouvenet N., Kochs G., Shoichet B., Ott M., Palmarini M., Shokat K. M., García-Sastre A., Rassen J. A., Grosse R., Rosenberg O. S., Verba K. A., Basler C. F., Vignuzzi M., Peden A. A., Beltrao P., Krogan N. J., (2020) Comparative host-coronavirus protein interaction networks reveal pan-viral disease mechanisms. Science, **370** (6521), eabe9403. https://doi.org/10.1126/science.abe9403.

Hao, W., Wojdyla, J. A., Zhao, R., Han, R., Das, R., Zlatev, I., Manoharan, M., Wang, M. and Cui, S. (2017) Crystal structure of Middle East respiratory syndrome coronavirus helicase. PLoS Pathog. **13**, e1006474.

Hillen, H. S., Kokic, G., Farnung, L., Dienemann, C., Tegunov, D. and Cramer, P. (2020) Structure of replicating SARS-CoV-2 polymerase. Nature **584**, 154–156.

Hoffmann H. H., Sánchez-Rivera F. J., Schneider W. M., Luna J. M., Soto-Feliciano Y. M., Ashbrook A. W., Le Pen J., Leal A. A., Ricardo-Lax I., Michailidis E., Hao Y., Stenzel A. F., Peace A., Zuber J., Allis C. D., Lowe S. W., MacDonald M. R., Poirier J. T., Rice C. M. (2021) Functional interrogation of a SARS-CoV-2 host protein interactome identifies unique and shared coronavirus host factors. Cell Host & Microbe, **29** (2), 267–280.e5. https://doi.org/10.1016/j.chom.2020.12.009.

Jiang H.-W., Zhang H.-N., Meng Q.-F., Xie J., Li Y., Chen H., Zheng Y.-X., Wang X.-N., Qi H., Zhang J., Wang P.-H., Han Z.-G., Tao S.-C. (2020) SARS-CoV-2 Orf9b suppresses type I interferon responses by targeting TOM70. Cellular & Molecular Immunology, **17** (9), 998–1000. https://doi.org/10.1038/s41423-020-0514-8.

Kaksonen, M., Toret, C. P. and Drubin, D. G. (2005) A modular design for the clathrin- and actin-mediated endocytosis machinery. Cell **123**, 305–320.

Kern, D. M., Sorum, B., Hoel, C. M., Sridharan, S., Remis, J. P., Toso, D. B. and Brohawn, S. G. (2020) Cryo-EM structure of the SARS-CoV-2 3a ion channel in lipid nanodiscs. bioRxiv, **6** (17), 156554. https://doi.org/10.1101/2020.06.17.156554.

Kim D.-K., Knapp J. J., Kuang D. A., Chawla A., Cassonnet P., Lee H., Sheykhkarimli D., Samavarchi-Tehrani P., Abdouni H., Rayhan A., Li R., Pogoutse O., Coyaud É., van der Werf S., Demeret C., Gingras A.-C., Taipale M., Raught B., Jacob Y., Roth F. P. (2020) A Comprehensive, Flexible Collection of SARS-CoV-2 Coding Regions. G3 Genes|Genomes|Genetics, **10** (9), 3399–3402. https://doi.org/10.1534/g3.120.401554.

Klein, S., Cortese, M., Winter, S. L., Wachsmuth-Melm, M., Neufeldt, C. J., Cerikan, B., Stanifer, M. L., Boulant, S., Bartenschlager, R. and Chlanda, P. (2020) SARS-CoV-2 structure and replication characterized by in situ cryo-electron tomography. Nat. Commun. **11**, 5885–10.

Kreimendahl S., Rassow J. (2020) The Mitochondrial Outer Membrane Protein Tom70-Mediator in Protein Traffic, Membrane Contact Sites and Innate Immunity. International Journal of Molecular Sciences, **21** (19), 7262. https://doi.org/10.3390/ijms21197262.

Laurent, E. M. N. et al. (2020) Global BioID-based SARS-CoV-2 proteins proximal interactome unveils novel ties between viral polypeptides and host factors involved in multiple COVID19-associated mechanisms. bioRxiv **2020.08.28.272955**. https://doi.org/10.1101/2020.08.28.272955.

Lee, S., Lim, W. A. and Thorn, K. S. (2013) Improved blue, green, and red fluorescent protein tagging vectors for S. cerevisiae. PLoS One **8**, e67902.

Lim, K. P. and Liu, D. X. (2001) The missing link in coronavirus assembly. Retention of the avian coronavirus infectious bronchitis virus envelope protein in the pre-Golgi compartments and physical interaction between the envelope and membrane proteins. J. Biol. Chem. **276**, 17515–17523.

Ma, Y., Wu, L., Shaw, N., Gao, Y., Wang, J., Sun, Y., Lou, Z., Yan, L., Zhang, R. and Rao, Z. (2015) Structural basis and functional analysis of the SARS coronavirus nsp14-nsp10 complex. Proc. Natl. Acad. Sci. U.S.A. **112**, 9436–9441.

Mandala V. S., McKay M. J., Shcherbakov A. A., Dregni A. J., Kolocouris A., Hong M. (2020) Structure and drug binding of the SARS-CoV-2 envelope protein transmembrane domain in lipid bilayers. Nat Struct Mol Biol, **27** (12), 1202–1208. https://doi.org/10.1038/s41594-020-00536-8.

Meier, C., Aricescu, A. R., Assenberg, R., Aplin, R. T., Gilbert, R. J. C., Grimes, J. M. and Stuart, D. I. (2006) The crystal structure of ORF-9b, a lipid binding protein from the SARS coronavirus. Struct. Fold. Des. **14**, 1157–1165.

Oudshoorn, D., Rijs, K., Limpens, R. W. A. L., Groen, K., Koster, A. J., Snijder, E. J., Kikkert, M. and Bárcena, M. (2017) Expression and cleavage of middle east respiratory syndrome coronavirus nsp3-4 polyprotein induce the formation of double-membrane vesicles that mimic those associated with coronaviral RNA replication. mBio **8**(6), e01658-17. https://doi.org/10.1128/mBio.01658-17.

Qu, Y. et al. (2020) ORF3a mediated-incomplete autophagy facilitates SARS-CoV-2 replication. bioRxiv **11** (12), 380709. https://doi.org/10.1128/mBio.01658-17.

Schoeman, D. and Fielding, B. C. (2019) Coronavirus envelope protein: current knowledge. Virol. J. **16**, 69–22.

Shang, J., Wan, Y., Luo, C., Ye, G., Geng, Q., Auerbach, A. and Li, F. (2020) Cell entry mechanisms of SARS-CoV-2. Proc. Natl. Acad. Sci. U.S.A. **117**, 11727–11734.

Shi, C.-S., Qi, H.-Y., Boularan, C., Huang, N.-N., Abu-Asab, M., Shelhamer, J. H. and Kehrl, J. H. (2014) SARS-coronavirus open reading frame-9b suppresses innate immunity by targeting mitochondria and the MAVS/TRAF3/TRAF6 signalosome. J. Immunol. **193**, 3080–3089.

Sicari, D., Chatziioannou, A., Koutsandreas, T., Sitia, R. and Chevet, E. (2020) Role of the early secretory pathway in SARS-CoV-2 infection. J. Cell Biol. **219**, e202006005.

Snijder, E. J., Limpens, R. W. A. L., de Wilde, A. H., de Jong, A. W. M., Zevenhoven-Dobbe, J. C., Maier, H. J., Faas, F. F. G. A., Koster, A. J. and Bárcena, M. (2020) A unifying structural and functional model of the coronavirus replication organelle: Tracking down RNA synthesis. PLoS Biol. **18**, e3000715.

St-Germain, J. R., Astori, A., Samavarchi-Tehrani, P., Abdouni, H., Macwan, V., Kim, D.-K., Knapp, J. J., Roth, F. P., Gingras, A.-C.

and Raught, B. (2020) A SARS-CoV-2 BioID-based virus-host membrane protein interactome and virus peptide compendium: new proteomics resources for COVID-19 research. bioRxiv **2020.08.28**, 269175. https://doi.org/10.1101/2020.08.28.269175.

Stukalov, A. & *et al*. (2020) Multi-level proteomics reveals host-perturbation strategies of SARS-CoV-2 and SARS-CoV. bioRxiv **2020.06.17**, 156455. https://doi.org/10.1101/2020.06.17.156455.

Subissi, L., Imbert, I., Ferron, F., Collet, A., Coutard, B., Decroly, E. and Canard, B. (2014) SARS-CoV ORF1b-encoded nonstructural proteins 12–16: replicative enzymes as antiviral targets. Antiviral Res. **101**, 122–130.

Tan, Y.-J., Teng, E., Shen, S., Tan, T. H. P., Goh, P.-Y., Fielding, B. C., Ooi, E.-E., Tan, H.-C., Lim, S. G. and Hong, W. (2004) A novel severe acute respiratory syndrome coronavirus protein, U274, is transported to the cell surface and undergoes endocytosis. J. Virol. **78**, 6723–6734.

Wolff G., Limpens R. W. A. L., Zevenhoven-Dobbe J.C., Laugks U., Zheng S., de Jong A. W. M., Koning R. I., Agard D. A., Grünewald K., Koster A. J., Snijder E. J., Bárcena M. (2020) A molecular pore spans the double membrane of the coronavirus replication organelle. Science, **369** (6509), 1395–1398. https://doi.org/10.1126/science.abd3629.

Zhang, J., Cruz-cosme, R., Zhuang, M.-W., Liu, D., Liu, Y., Teng, S., Wang, P.-H. and Tang, Q. (2020) A systemic and molecular study of subcellular localization of SARS-CoV-2 proteins. bioRxiv **2020.08.02**, 233023. https://doi.org/10.1101/2020.08.02.233023.

Zhong, X., Guo, Z., Yang, H., Peng, L., Xie, Y., Wong, T.-Y., Lai, S.-T. and Guo, Z. (2006) Amino terminus of the SARS coronavirus protein 3a elicits strong, potentially protective humoral responses in infected patients. J. Gen. Virol. **87**, 369–373.

Freundt E. C., Yu L., Goldsmith C. S., Welsh S., Cheng A., Yount B., Liu W., Frieman M. B., Buchholz U. J., Screaton G. R., Lippincott-Schwartz J., Zaki S. R., Xu X.-N., Baric R. S., Subbarao K., Lenardo M. J. (2010) The Open Reading Frame 3a Protein of Severe Acute Respiratory Syndrome-Associated Coronavirus Promotes Membrane Rearrangement and Cell Death. J. Virol., **84** (2), 1097–1109. https://doi.org/10.1128/jvi.01662-09.

Yue Y., Nabar N. R., Shi C.-S., Kamenyeva O., Xiao X., Hwang I.-Y., Wang M., Kehrl J. H. (2018) SARS-Coronavirus Open Reading Frame-3a drives multimodal necrotic cell death. Cell Death & Disease, **9** (9), https://doi.org/10.1038/s41419-018-0917-y.